Journal of Physics: Photonics



OPEN ACCESS

RECEIVED
7 January 2026

REVISED
26 February 2026

ACCEPTED FOR PUBLICATION
16 March 2026

PUBLISHED
23 March 2026



LETTER

# Suppression of frequency splitting induced by weak anisotropy via construction of anti-parity-time symmetry in polarization space

**Gang Huang**[1,2], **Pengfei Zhou**[1,3], **Yongcheng Huang**[1,2], **Bingxuan Li**[1,4,*] and **Ge Zhang**[1,4,*]

[1] State Key Laboratory of Functional Crystals and Devices, Fujian Institute of Research on the Structure of Matter, Chinese Academy of Sciences, Fuzhou, Fujian, People's Republic of China
[2] University of Chinese Academy of Sciences, Beijing, People's Republic of China
[3] Fujian Normal University, Fuzhou, Fujian, People's Republic of China
[4] Fujian Science & Technology Innovation Laboratory for Optoelectronic Information of China, Fuzhou, Fujian, People's Republic of China
[*] Authors to whom any correspondence should be addressed.

**E-mail:** libingxuan@fjirsm.ac.cn and zhg@fjirsm.ac.cn

**Keywords:** anti-PT symmetric, frequency degeneracy, polarization space

## Abstract

From optical sensors to precision measurement, modern photonic systems are demonstrating heightened sensitivity to even slight frequency splitting between polarization eigenmodes. Nevertheless, the inherent weak anisotropy of the crystal inevitably induces such splitting. Here, we demonstrate that such frequency splitting can be suppressed by constructing an anti-parity-time (PT) symmetry system in polarization space. In a laser system with weak anisotropy, we observe the transition from splitting to degeneracy in the frequency domain as the system enters the exact anti-PT-symmetric phase, consistent with a non-Hermitian two-component system. Our results reveal a physical mechanism by which anti-PT symmetry counteracts weak anisotropies without requiring complex control schemes. This approach offers a compact and intrinsically self-balancing pathway toward polarization stabilization, with potential applications in integrated optical sensors, topological photonic systems, and quantum photonic systems.

## 1. Introduction

Frequency degeneracy in optical resonators supports rich spatial mode structures [1, 2] and plays a crucial role in enhancing the sensitivity and resolution of precision sensing systems [3, 4]. In particular, nanoparticle detection [5–7] and the study of quantum noise [8] often require single-frequency laser operation, as both spectral purity and mode coherence are critical for achieving high sensitivity and avoiding signal ambiguity [9]. However, even weak anisotropies arising from the gain medium, cavity mirrors, or thermal birefringence can inevitably lead to frequency splitting between orthogonal polarization eigenmodes. Conventional methods to mitigate frequency splitting typically rely on active feedback or elaborate polarization control elements, which increase system complexity and reduce integration potential.

Optical resonators are intrinsically non-Hermitian systems due to unavoidable diffraction loss and absorption. In such systems, dissipation is not merely a loss mechanism but can actively reshape the eigenvalue spectrum [10, 11]. A particularly important consequence of non-Hermiticity is that spectral properties are strongly constrained by symmetry, which can be exploited to engineer frequency degeneracies. Therefore, by tailoring the symmetry of the effective non-Hermitian Hamiltonian, it becomes possible to suppress frequency splitting induced by weak anisotropies.

Among various non-Hermitian systems, parity-time (PT) symmetry has been widely explored in real spatial photonic platforms. A PT-symmetric system satisfies a combined parity and time-reversal invariance, which can give rise to entirely real eigenvalue spectra despite non-Hermiticity [12–14]. A key feature of PT-symmetric systems is the existence of exceptional points (EPs), where both eigenvalues and

eigenvectors coalesce, separating an exact PT-symmetric phase from a broken PT-symmetric phase [15–17]. The eigenvalues are entirely real in the exact PT symmetric phase, and the eigenvalue spectrum becomes complex conjugate in the broken phase, where the real and imaginary parts of the eigenvalues correspond respectively to the eigenmode frequency and the net gain or loss. Conventionally, realizing optical PT symmetry requires constructing a complex potential $V(\vec{r}) = V^*(-\vec{r})$, which translates to a strict constraint on the refractive index distribution: $n_r(x) + in_i(x) = n_r(-x) - in_i(-x)$. Achieving this in spatial domains often demands precise material processing to balance gain and loss regions [18, 19].

Recently, PT symmetry has been constructed in the polarization space by adjusting the Jones matrix to commute with the PT operator [20–22], and it can be achieved by employing anisotropic mirrors combined with quarter-wave plates in the laser resonator [23]. This approach offers a more convenient and flexible way to realize PT symmetry. However, PT symmetry fundamentally characterizes the dynamical evolution of the system, it should be associated with the operator of evolution rather than inferred from a static matrix. The periodicity of modal evolution in a laser resonator is properly accounted for within the Floquet framework, the effective Hamiltonian of a Fabry–Pérot (FP) cavity in polarization space naturally acquires an anti-PT-symmetric structure. Both the PT symmetry and the anti-PT symmetry provide a direct correspondence between spectral properties and experimentally accessible observables [24, 25]. In particular, anti-PT symmetry exhibits a PT-symmetric-like spectral structure, including EPs, spontaneous symmetry-breaking transition, and self-intersecting spectral topology, leading to continuous lasing spectra [26], refraction-less propagation [27, 28], flat all-pass transmission bands [29], and scattering characteristics dictated by scattering centers [30]. Moreover, in contrast to PT-symmetry, the exact anti-PT-symmetric phase supports frequency-degenerate polarization eigenmodes with unequal amplitudes, while the broken phase induces a frequency splitting between orthogonally polarized eigenmodes.

In this letter, we establish a rigorous Floquet description of anti-PT symmetry in the polarization space of a FP cavity. We demonstrate that the frequency splitting caused by inherent weak anisotropy can be effectively suppressed in the exact anti-PT-symmetric phase. By adjusting the loss difference between the polarization eigenmodes, the system can be tuned from the anti-PT symmetry broken phase into the exact anti-PT symmetry phase, thereby suppressing the frequency splitting of the polarization eigenmodes without the active feedback modulation or the insertion of additional optical components. Our results provide a physically transparent framework for analyzing polarization eigenmode dynamics in laser resonators and offer a practical route for mitigating frequency splitting induced by weak anisotropy.

## 2. Anti-PT-symmetric construction in polarization space

In general, a Hamiltonian $\hat{H}$ is anti-PT-symmetric provided that it anti-commutes with the $\mathcal{PT}$ operator. Here, the parity operator $\mathcal{P}$, which performs spatial inversion, is represented by the Pauli matrix $\sigma_x$, while the time-reversal operator $\mathcal{T}$ corresponds to complex conjugation.

Consider a non-Hermitian two-component system. A simplest Hamiltonian that satisfies this condition can be described by a $2 \times 2$ matrix [31, 32]:

$$\hat{H} = \hbar \begin{pmatrix} -\omega + i\gamma & i\kappa \\ i\kappa & \omega + i\gamma \end{pmatrix}, \tag{1}$$

where the diagonal elements represent two modes at frequencies $\pm\omega$ that experience a common uniform gain/loss background $\gamma$, and the off-diagonal elements $i\kappa$ describe purely imaginary coupling between the two modes.

The eigenvalues of this Hamiltonian can be derived as

$$\lambda_{\pm} = \hbar \left( i\gamma \pm \sqrt{\omega^2 - \kappa^2} \right), \tag{2}$$

where the real part corresponds to the energy levels of the system, and the imaginary part characterizes the gain/loss experienced by the eigenstate. Physically, the eigenvalues represent the complex resonance frequencies in a laser system, the real part corresponds to the resonance frequency or the phase accumulation per round trip, and the imaginary part characterizes the gain/loss similarly.

According to equation (2), the spectral properties and symmetry of the system are determined by the relationship between $\omega$ and $\kappa$. As illustrated in figure 1(a), when $|\kappa| < |\omega|$, the eigenvalues acquire unequal real parts, indicating a frequency splitting between the eigenmodes. In contrast to conventional PT-symmetric systems, such real part splitting typically appears in the broken anti-PT-symmetric phase.

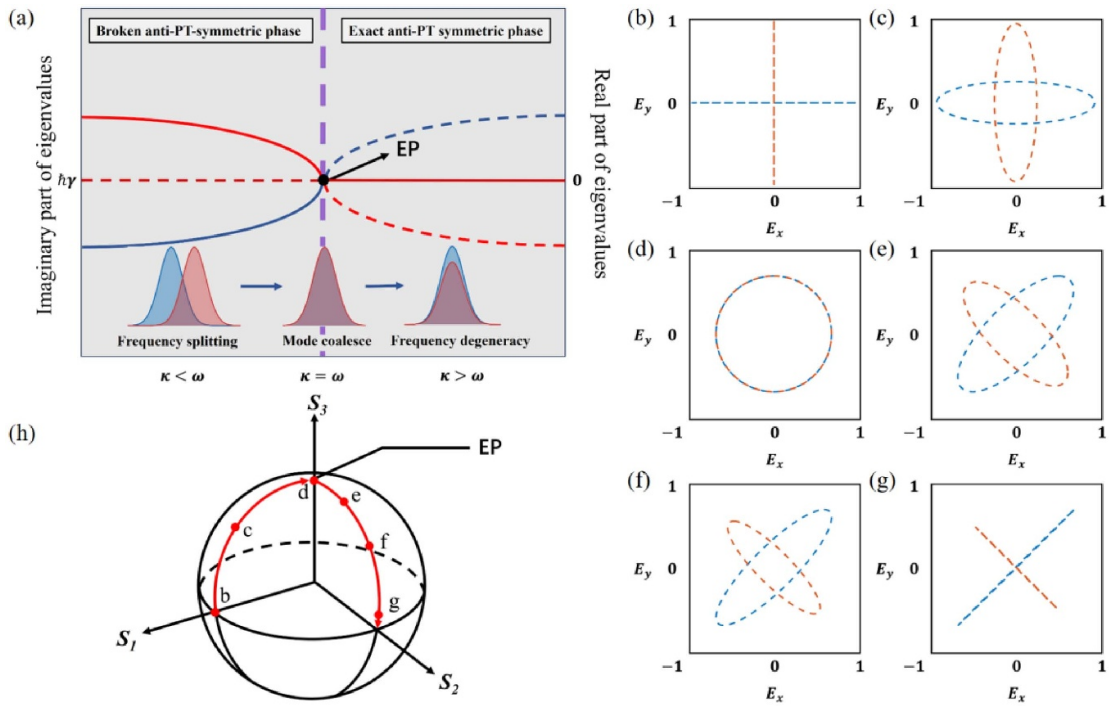


**Figure 1.** (a) Eigenvalue spectrum of the anti-PT-symmetric Hamiltonian. The red curves and the blue curves correspond to the specific component. Solid lines denote the real parts of the eigenvalues, while dashed lines represent the imaginary parts. When $|\kappa| < |\omega|$, the system resides in the broken anti-PT-symmetric phase, characterized by frequency splitting of the eigenmodes. At $|\kappa| = |\omega|$, an EP emerges where both eigenvalues and eigenvectors coalesce. For $|\kappa| > |\omega|$, the system enters the exact anti-PT-symmetric phase, where the eigenvalues are purely imaginary, leading to degenerate resonance frequencies with unequal amplitudes. (b)–(g) Evolution of the polarization eigenmodes in the polarization space as the system is tuned across the EP: (b) orthogonal linearly polarized modes in the broken phase; (c) orthogonal elliptically polarized modes approaching the EP; (d) coalesced circularly polarized mode at the EP; (e) and (f) bifurcation into orthogonal elliptically polarized modes in the exact phase; (g) orthogonal linearly polarized modes in the exact phase. (h) Continuous evolution trajectory of a representative eigenmode on the Poincaré sphere from the broken to the exact anti-PT-symmetric phase.

As $\kappa$ approaches $\omega$, the system reaches an EP, at which both the eigenvalues and their associated eigenvectors coalesce. At this critical point, the Hamiltonian becomes non-diagonalizable, marking the boundary between the broken and exact anti-PT-symmetric phases. For $|\kappa| > |\omega|$, the system enters the exact anti-PT-symmetric phase, and the Hamiltonian satisfies the anti-commutation relation $\{\hat{H}, \mathcal{PT}\} = 0$. In this regime, the eigenvalues are purely imaginary, and thus the resonance frequencies of the eigenmodes become degenerate. Moreover, the amplitudes of the eigenmodes differ due to the inconsistency of the imaginary parts.

A natural realization of such a laser system is the polarization space. For convenience and experimental accessibility, the horizontal and vertical polarization components are adopted as an orthogonal basis here. Within this framework, the evolution of the polarization orientations of the eigenmodes in relation to the symmetry of the system can be directly visualized by tracking the eigenvectors associated with the eigenvalues. In the broken anti-PT-symmetric phase, the system initially supports a pair of orthogonal linearly polarized eigenmodes with frequency splitting, as shown in figure 1(b). As the system parameters are continuously tuned toward the EP, evolve into a pair of orthogonal elliptically polarized modes as shown in figure 1(c). At EP, two eigenmodes coalesce into an indistinguishable circularly polarized mode, as shown in figure 1(d), reflecting the simultaneous merging of both eigenvalues and eigenvectors. Upon crossing the EP into the exact anti-PT-symmetric phase, the circular polarization bifurcates again into two orthogonal elliptically polarized modes as shown in figures 1(e), (f), and further evolves into orthogonal linear polarizations figure 1(g). Notably, the major axes of the polarization ellipses will be rotated by 45° with respect to the linear polarization in the broken-symmetry regime. Figure 1(h) illustrates the continuous evolution trajectory of one representative eigenmode on the Poincaré sphere as the system is tuned from the broken phase to the exact anti-PT-symmetric phase.

For laser systems that are inherently time-periodic in nature, the Hamiltonian $\hat{H}(t)$ satisfies $\hat{H}(t+T) = \hat{H}(t)$, where $T$ denotes the period. According to Floquet theory, the evolution over one period is governed by the unitary operator [33, 34]:

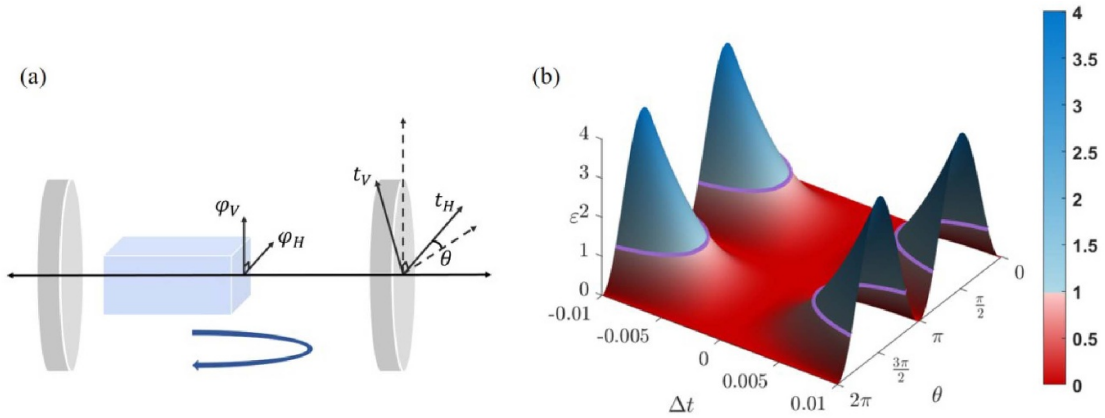


**Figure 2.** (a) Schematic of the FP cavity with an isotropic gain medium. Weak birefringence in the cavity introduces a round-trip phase accumulation for the horizontal ($\varphi_{\mathrm{H}}$) and vertical ($\varphi_{\mathrm{V}}$) polarization eigenmodes. A slight tilt of the output coupler mirror gives rise to polarization-dependent transmittances $t_{\mathrm{H}}$ and $t_{\mathrm{V}}$ according to Fresnel's equations, leading to anisotropic output coupling losses. And the principal axes of phase anisotropy (associated with birefringence) are rotated by an angle $\theta$ relative to the principal axes of loss anisotropy. (b) The parametrically controlled PT-symmetry phase diagram scans across $\Delta t \in [-0.01, 0.01]$ and $\theta \in [0, \pi]$ at fixed $\Delta\varphi = 0.005$. The blue regions ($\varepsilon > 1$) correspond to the exact anti-PT-symmetric phase, the red region ($\varepsilon < 1$) is the broken anti-PT-symmetric phase, and the critical purple line ($\varepsilon = 1$) represents the exceptional line.

$$U(t_0+T, t_0) = \exp\left(-\frac{i}{\hbar}\int_{t_0}^{t_0+T} \hat{H}(t)\,\mathrm{d}t\right) \equiv e^{-iH_{\mathrm{eff}}T/\hbar}, \tag{3}$$

where $H_{\mathrm{eff}}$ is a time-independent Hermitian operator, the so-called effective Hamiltonian. The Floquet evolution operator can be described by a Jones matrix in polarization space, which characterizes the propagation and transformation of polarization states through an optical component or medium. As shown in figure 2(a), we construct a model of a laser system of an isotropic gain medium within an FP cavity. The weak birefringence inevitably arises from residual stress, temperature gradients, or structural imperfections, resulting in a different phase accumulation for the orthogonal polarization eigenmodes. We denote the phase difference in per round trip introduced by this birefringence as $\Delta\varphi = \varphi_{\mathrm{H}} - \varphi_{\mathrm{V}}$, where $\varphi_{\mathrm{H}}$ and $\varphi_{\mathrm{V}}$ represent the phase accumulation for the horizontal and vertical polarization eigenmodes, respectively. Moreover, a slight tilt in the cavity mirrors introduces anisotropic losses between polarization eigenmodes. According to Fresnel's laws, the polarization-dependent transmittances in a cavity can be approximately estimated using the Fresnel equations:

$$\begin{aligned} t_{\mathrm{H}} &= 1 - \left(\frac{\cos\theta_t - n_2\cos\theta_i}{\cos\theta_t + n_2\cos\theta_i}\right)^2, \\ t_{\mathrm{V}} &= 1 - \left(\frac{\cos\theta_i - n_2\cos\theta_t}{\cos\theta_i + n_2\cos\theta_t}\right)^2, \end{aligned} \tag{4}$$

where $t_{\mathrm{H}}$ and $t_{\mathrm{V}}$ represent the transmittance for horizontal polarization and vertical polarization, respectively; $\theta_i$ and $\theta_t$ denote the incidence and refraction angles of the laser, and $n_2$ is the refractive index of the output coupler (OC) mirror substrate. In the context of cavity round-trip evolution, the polarization-dependent transmittances directly correspond to output coupling losses. Consequently, the angle-dependent transmission imbalance introduced by the OC mirror can be equivalently regarded as an effective anisotropic loss inside the cavity, and denote the differential loss as $\Delta t = (t_{\mathrm{H}} - t_{\mathrm{V}})/2$. It is important to note that the coordinate system associated with phase anisotropy is rotated by an angle $\theta$ with respect to the principal axes of the loss anisotropy. Taking these effects into account, a round-trip evolution of the polarization eigenmodes can be described by the following Jones matrix $M$[35, 36]:

$$\begin{aligned} M &= \begin{pmatrix} e^{-i\Delta\varphi} & 0 \\ 0 & 1 \end{pmatrix}\begin{pmatrix} \cos\theta & \sin\theta \\ -\sin\theta & \cos\theta \end{pmatrix}\begin{pmatrix} 1+\Delta t & 0 \\ 0 & 1-\Delta t \end{pmatrix}\begin{pmatrix} \cos\theta & -\sin\theta \\ \sin\theta & \cos\theta \end{pmatrix}\begin{pmatrix} 1 & 0 \\ 0 & e^{i\Delta\varphi} \end{pmatrix} \\ &= \begin{pmatrix} (1+\cos 2\theta\Delta t)\,e^{-i\Delta\varphi} & -\sin 2\theta\Delta t \\ -\sin 2\theta\Delta t & (1+\cos 2\theta\Delta t)\,e^{i\Delta\varphi} \end{pmatrix} \\ &= \begin{pmatrix} ae^{-i\Delta\varphi} & b \\ b & ae^{i\Delta\varphi} \end{pmatrix}, \end{aligned} \tag{5}$$

where $a = 1 + \cos 2\theta\Delta t$, $b = \sin 2\theta\Delta t$. By setting $\hbar = 1$, the effective Hamiltonian can be consequently defined via the relation:

$$M = e^{-iH_{\text{eff}}T} \rightarrow H_{\text{eff}} = \frac{i}{T}\ln M. \tag{6}$$

Note that the eigenvalues of $M$ can be derived by equation (5):

$$\lambda_{1,2} = a\cos\Delta\varphi \pm \sqrt{b^2 - a^2\sin^2\Delta\varphi}. \tag{7}$$

Therefore, the effective Hamiltonian can be derived:

$$H_{\text{eff}} = \frac{1}{2T\Gamma}\begin{pmatrix} ax_1\sin\Delta\varphi + i\Gamma x_2 & ibx_1 \\ ibx_1 & -ax_1\sin\Delta\varphi + i\Gamma x_2 \end{pmatrix}, \tag{8}$$

where $x_1 = \ln\lambda_1 - \ln\lambda_2$, $x_2 = \ln\lambda_1 + \ln\lambda_2$ and $\Gamma = \sqrt{b^2 - a^2\sin^2\Delta\varphi}$. It is evident that the effective Hamiltonian shares the same mathematical form as $\hat{H}$ in equation (1). And the eigenvalues of $H_{\text{eff}}$ can be conveniently expressed as:

$$\lambda_{\text{eff},\pm} = \frac{i}{T}\ln(\lambda_{1,2}) = \frac{i}{T}\left(\ln\sqrt{\text{Re}^2(\lambda_{1,2}) + \text{Im}^2(\lambda_{1,2})} + i\arg(\lambda_{1,2})\right). \tag{9}$$

It can be seen that the spectral properties and symmetry of the system are determined by the eigenvalues of the Jones matrix $M$ and are independent of the particular choice of basis. The system exhibits anti-PT symmetry when $\arg(\lambda_{1,2}) = 0$, under which the eigenvalues of $H_{\text{eff}}$ are purely imaginary, implying that $\lambda_{1,2}$ are real. When $\lambda_{1,2}$ becomes degenerate, the system reaches an EP and polarization eigenmodes coalesce. In contrast, when $\lambda_{1,2}$ form a pair of complex-conjugate eigenvalues, the system enters the broken anti-PT-symmetric phase. Thus, the above expression motivates defining the coefficient $\varepsilon$ to characterize the anti-PT-symmetric property of the system:

$$\varepsilon = \frac{b^2}{a^2\sin^2\Delta\phi}. \tag{10}$$

That is, when $\varepsilon > 1$, the eigenvalues of the Jones matrix exhibit real and distinct values in the mathematical sense, indicating that the system exhibits anti-PT symmetry and emits a pair of orthogonal polarizations with identical frequency but different amplitudes. In contrast, $\varepsilon < 1$ signifies spontaneous anti-PT-symmetry breaking. As a result, the system emits orthogonal modes with the same amplitudes but different frequencies. Additionally, at the EP where $\varepsilon = 1$, eigenvalue degeneracy and state coalesce, fundamentally arising from the Jordan block structure of $M$, making it no longer diagonalizable. In other words, we can scan the exact and broken anti-PT-symmetry regions by tuning $\Delta t$ and $\theta$ at fixed $\Delta\varphi$, and avoid native frequency splitting caused by the weak anisotropy in the exact anti-PT-symmetry region. This dual-parameter adjustment extends the EP into an exceptional line.

Figure 2(b) systematically visualizes the anti-PT-symmetry phase diagram through a parametric surface defined by $\Delta t \in [-0.01, 0.01]$ and $\theta \in [0, \pi]$ at fixed $\Delta\varphi = 0.005$. The color gradient represents the interval of $\varepsilon$, where the deep blue regions ($\varepsilon > 1$) exhibit frequency degeneracy, corresponding to the exact anti-PT-symmetric phase, red regions ($\varepsilon < 1$) display complex-conjugate eigenvalues, marking the broken phase. The critical purple line ($\varepsilon = 1$) traces the exceptional line. This numerical model suggests that the transition occurs when the loss difference $\Delta t$ exceeds the phase accumulation $\Delta\varphi$ when projected into the same coordinate space.

## 3. Anti-PT symmetry observed in polarization space

The experimental setup of the laser system is illustrated in figure 3(a). A fiber-coupled 940 nm laser diode (numerical aperture = 0.22, core diameter = 200 $\mu$m) without polarization characteristics was employed as the pump source. The pump beam was collimated by a plano-convex lens pair with a coupling ratio of 2:1. The resonator was configured as an FP cavity, in which the pump mirror was coated with high transmission (HT) at 940 nm and high reflection (HR) at 1030/1050 nm The OC mirror had transmissions of 5.6 % and 4.2 % at 1030 nm and 1050 nm, respectively. The gain medium was a $4 \times 4 \times 5$ mm, 5 at. % Yb:YAG crystal with a $< 111 >$ cut, and the cavity length was fixed at 25 mm. The crystal was wrapped in indium foil and mounted on a water-cooled copper block, maintaining a temperature of approximately 287.9 K. A Glan prism (transmission range: 350–2300 nm) and a power

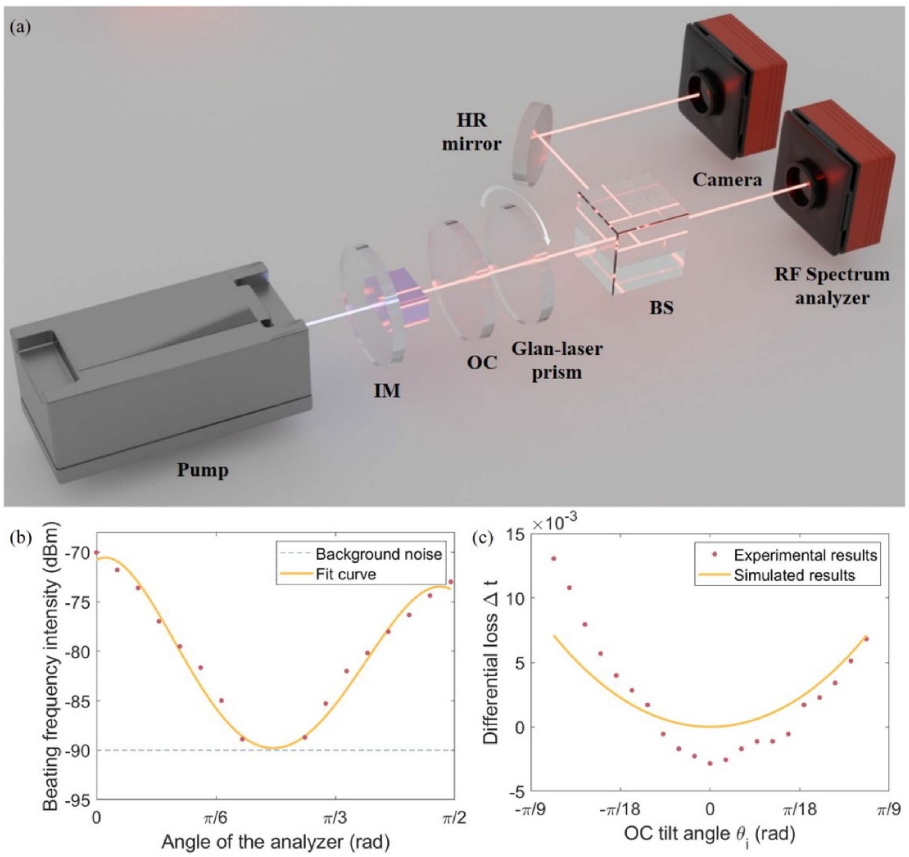


**Figure 3.** (a) Schematic diagram of experimental setup. (b) The intensity of the beating frequency varies with the rotation angle of the Glan prism when the beating frequency is 82.22 MHz. (c) The variation of the differential loss with the tilt angle of OC ranges from $-20°$ to $20°$. The spot represents the experimental results, and the solid line denotes the simulated results.

meter (Gentec-EO, Canada) were placed after the OC to analyze the polarization characteristics of the emitted laser. The beam profile was recorded by a CCD (DataRay, USA). After a beam splitter (BS), the frequency beating due to polarization-state variations was monitored using an RF signal spectrum analyzer (Siglent SSA5083A, bandwidth: 9 kHz–13.6 GHz).

Although Yb:YAG is classified within the cubic crystal system, internal defects or thermal expansion can induce weak anisotropy in the crystal. This anisotropy induces different phase accumulations for the eigenmodes during each round trip. Such phase accumulation $\varphi$ can be quantitatively related to the angular frequency of the eigenmodes by the relation $\omega = \mathrm{d}\varphi/\mathrm{d}t$. And the frequency splitting $\Delta f = |\omega_1 - \omega_2|/2\pi$ can be observed with the RF signal analyzer. Specifically, the beat frequency is given by:

$$\Delta f = \frac{1}{2\pi}\left|\mathrm{Re}\left(\lambda_{\mathrm{eff},+}\right) - \mathrm{Re}\left(\lambda_{\mathrm{eff},-}\right)\right| = \frac{1}{\pi T}\arg\left(\lambda_{1,2}\right). \tag{11}$$

We observed a beating frequency near 82.22 MHz, indicating that the laser system operates in the broken anti-PT-symmetric phase. By rotating the Glan prism, we can see how the beating frequency intensity changes with the rotation angle of the analyzer. As shown in figure 3(b), with the change of the rotation angle, the beating frequency intensity decreases continuously and disappears (not exceeding the average noise intensity). The intensity varies from maximum to indistinguishable from the background noise with the detecting angle range of $\pi/4$, and increases to maximum in the next $\pi/4$ range. The angular dependence of the beating frequency intensity excludes the possibility that the signal arises from the transverse mode beating. And this could well prove our previous hypothesis of the existence of a pair of orthogonal polarizations emerging from the weak anisotropies in the laser resonator. In this case, we should point out that the frequency difference between them will not change with the detection angle. When the RF direction coincides with a certain polarization, since the component of the other polarization direction is almost nothing, the beating intensity of these two modes should be near zero. When the angle between the RF direction and the polarization direction is $\pi/4$, the components of the two polarization modes in the RF direction are equal, and then the intensity of the beating signal should be the largest.

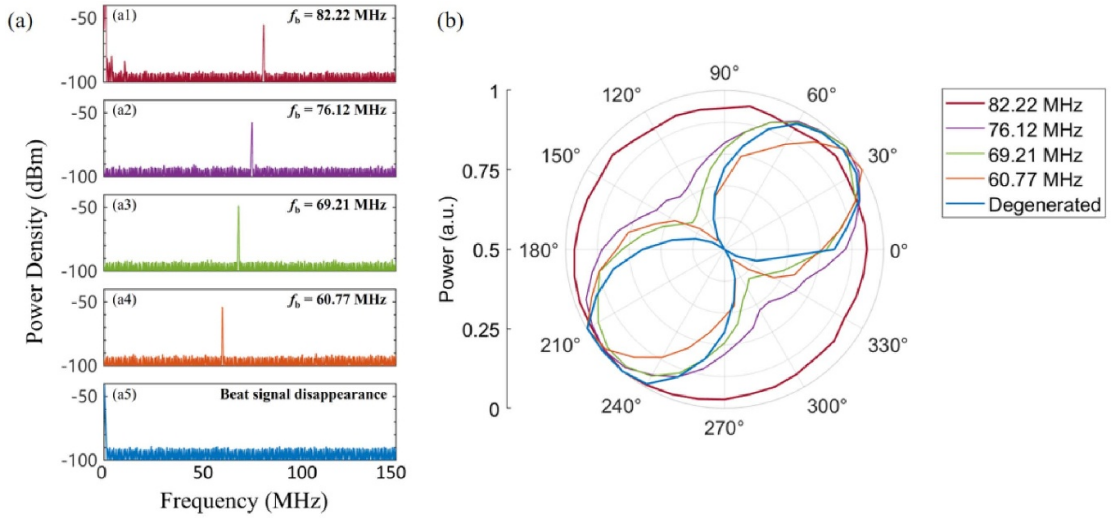


**Figure 4.** (a1)–(a5) RF spectra of the beat signal between the two polarization eigenmodes as the OC tilt angle is continuously increased. The beat frequency progressively decreases with tuning the differential loss and eventually becomes indistinguishable from the background noise. The disappearance of the beat signal signifies frequency degeneracy at the EP and the subsequent transition from the broken anti-PT-symmetric phase to the exact anti-PT-symmetric phase. (b) Polarization-resolved power measurements obtained by rotating a linear analyzer in front of the power meter; the polar angle denotes the orientation of the analyzer relative to the horizontal axis.

The OC mirror is mounted on a high-precision rotation stage. By rotating the OC mirror about the horizontal axis, the tilt angle $\theta_i$ is varied continuously from $-20^\circ$ to $20^\circ$, thereby enabling tunable polarization-dependent transmittances as governed by equation (4), and $\Delta t$ can therefore be continuously tuned. The dependence of the differential loss on the tilt angle is shown in figure 3(c). The spot represents the experimental results, while the solid line corresponds to the theoretical prediction based on Fresnel equations, assuming a refractive index $n_2 = 1.5$ and a normal-incidence transmittance of 1 %.

The continuous tunability of the differential loss enables the system to transition from the broken anti-PT-symmetric phase to the exact anti-PT-symmetric phase. The beating frequency between the polarization eigenmodes was used to monitor the evolution of the system during the tuning process. With increasing tilt angle of the OC, the frequency difference gradually decreases, as shown in figures 4(a1)–(a4) and eventually becomes indistinguishable from the background noise in figure 4(a5). The disappearance of the beating frequency indicates the frequency splitting is suppressed, marking the transition from the broken anti-PT-symmetry phase to the EPs and finally entering the exact anti-PT-symmetric phase.

Simultaneous polarization-resolved power measurement further reveals the evolution of the eigenmodes as the system transitions from the broken phase to the exact symmetric phase. As shown in figure 4(b), the measurements were performed by placing an analyzer in front of the power meter, polar coordinates denote the angle between the polarization direction and the horizontal direction. In the broken phase, where the eigenmodes possess distinct frequencies, the detected signal corresponds to a long-time average, and the measured polarization distribution is governed solely by the relative modal intensities. When the beat signal is 82.22 MHz, the orthogonal polarization eigenmodes exhibit nearly net gain, resulting in a low polarization contrast and an almost isotropic power distribution. As the OC tilt angle is further tuned and the system approaches the exact anti-PT symmetric phase, the beat signal decreases from 82.22 MHz to 60.77 MHz, corresponding to the reduction in the real-part splitting of the eigenvalues of the effective Hamiltonian. In this regime, the system becomes increasingly sensitive to small loss differences. As a result, even a slight imbalance in cavity loss is magnified, and one eigenmode begins to dominate in intensity. This produces an increasingly linear polarization component in the time-averaged power distribution. Until the system enters the exact anti-PT-symmetric phase, the initially unpolarized emission evolves into a linearly polarized beam with high purity, characterized by a polarization extinction ratio exceeding 26.91 dB. This polarization state resulted from the frequency degeneracy of the orthogonal polarization eigenmodes, which coalesced into a single linearly polarized mode.

Notably, even in the exact anti-PT-symmetric phase where the frequency degeneracy, both polarization eigenmodes remain supported by the cavity, the observed high extinction ratio reflects the stabilized

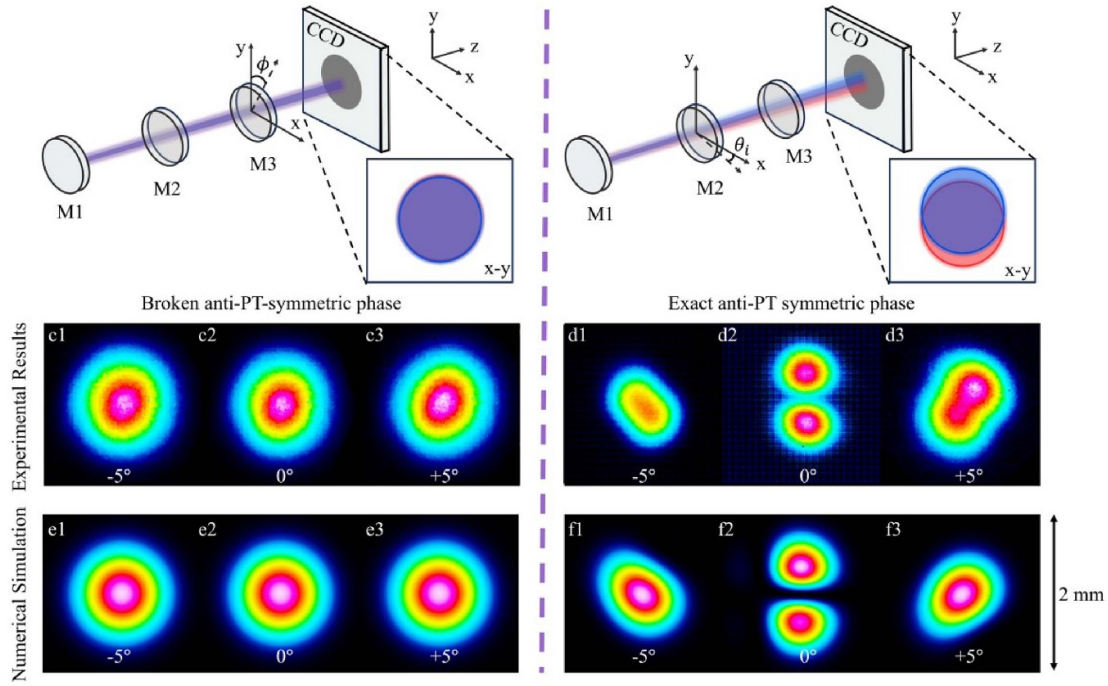


**Figure 5.** Spatial characteristics of the polarization eigenmodes in the broken and exact anti-PT-symmetric phases. (a), (b) Schematic diagrams of the corresponding experimental configurations, where M1 represents the pump mirror, M2 is OC, and M3 is the Glan prism. In (a), corresponding to the broken anti-PT-symmetric phase, the two polarization components spatially overlap. In (b), corresponding to the exact anti-PT-symmetric phase, the two polarization eigenmodes exhibit spatial separation. (c), (d) Measured beam profiles in the broken and exact anti-PT-symmetric phases, respectively. (e), (f) Numerical simulations incorporating birefringence-induced beam center walk-off with a displacement between the two Gaussian beams. Simulation parameters: $\omega_{x,H/V} = 0.29$ mm, $\omega_{y,H/V} = 0.30$ mm, with relative center displacement $(\Delta x, \Delta y) = (4, 13)\,\mu$m.

phase relation and modal superposition rather than the complete suppression of one mode. And this can be demonstrated by the spatial characteristics of the eigenmodes.

Figures 5 shows the spatial characteristics of the polarization eigenmodes in both the anti-PT broken and symmetric phases. Figures 5(a) and (b) show the corresponding experimental configurations. In both cases, the output beam from an FP cavity is analyzed by a rotatable Glan prism and recorded by a CCD. The Glan prism transmission axis forms an angle $\phi$ with respect to the vertical direction. And the OC is mounted on a horizontal tilt stage with tilt angle $\theta_i$, enabling tuning across the phase transition.

The measured beam profiles are summarized in figures 5(c) and (d). In the symmetric phase, where the two eigenmodes are frequency-degenerate and form a coherent superposition, the extinction angle is determined from the polarization-resolved power measurement as shown in figure 4(b) and defined as 0°. The corresponding CCD images recorded at 0° and at ±5° relative to extinction are labeled d2, d1, and d3 in figure 5(d). At the extinction position, two residual intensity spots remain visible. When the analyzer is rotated by ±5°, the beam profiles evolve into two elliptical spots whose major axes are nearly orthogonal. This phenomenon arises because the spatial distributions of the two orthogonal eigenmodes do not fully overlap. Since the modes are frequency-degenerate, the overlapping region coherently superimposes into a single linearly polarized beam, while the non-overlapping regions preserve the polarization states of the original eigenmodes. For comparison, figure 5(c) shows the beam patterns in the broken anti-PT-symmetric phase. In this case, the laser system emitted a nearly circular spot, and no significant changes were observed by adjusting the angle of the analyzer. The extinction position (c2) exhibits a more uniform suppression of the beam, and the profiles at ±5° (c1 and c3) display symmetric modulation consistent with a coherently superimposed linear polarization.

Accounting for beam center walk-off due to birefringence, with the displacement between two Gaussian beam centers set to $(\Delta x, \Delta y) = (4, 13)\mu$m, numerical simulations incorporating complete and partial spatial overlap are presented in figures 5(e) and (f), corresponding to the experimental results in figures 5(c) and (d), respectively. Due to the unavoidable factors, such as thermal lensing effects in the Yb:YAG crystal and slight wavefront aberrations, the beam shape can be distorted. Despite these deviations, the simulations reproduce the residual dual-spot structure observed at extinction and confirm that the observed features arise from incomplete spatial overlap of the two orthogonal polarization eigenmodes, rather than from the disappearance of one mode.

## 4. Conclusion

In summary, we have demonstrated the realization of anti-PT symmetry in the polarization space within the framework of Floquet theory. By treating the polarization-dependent losses as tunable parameters, we constructed a non-Hermitian system whose dynamics are governed by the effective Hamiltonian. Theoretical analysis confirmed that the natural frequency splitting caused by weak anisotropies can be suppressed in the exact anti-PT-symmetry phase. Spectral measurement and the observation of beam profiles experimentally confirm suppression of the natural frequency splitting and the superposition of the eigenmodes in the exact anti-PT-symmetry phase, simultaneously revealing single-frequency emission with linear polarization. Remarkably, we extend anti-PT-symmetry concepts to polarization degrees of freedom, offering a method to suppress frequency splitting without active feedback, with potential applications in quantum-limited sensing and integrated photonics.

## Funding

Youth Innovation Promotion Association CAS (2022 303), CAS Key Technology Talent Program (2022000061), the Self-deployment Project Research Program of Haixi Institutes, Chinese Academy of Sciences (CXZX-2023-JQ01, CXZX-2022-GH09), National Natural Science Foundation of China (U21A20508), Fujian Science & Technology Innovation Laboratory for Optoelectronic Information of China (2024CXY108, 2020ZZ108, and 2021ZZ118), and the STS Project of Fujian-CAS (2024T3009).

## Data availability statement

All data that support the findings of this study are included within the article (and any supplementary files).

## Author contributions

Gang Huang
Conceptualization (lead), Formal analysis (lead), Methodology (lead), Software (lead), Visualization (lead), Writing – original draft (lead)

Pengfei Zhou
Investigation (lead), Methodology (equal), Validation (lead)

Yongcheng Huang
Formal analysis (supporting), Investigation (supporting)

Bingxuan Li 0000-0002-6921-3448
Funding acquisition (equal), Writing – review & editing (equal)

Ge Zhang 0000-0002-0849-0521
Conceptualization (supporting), Funding acquisition (equal), Project administration (lead), Resources (lead), Supervision (lead), Writing – review & editing (equal)

## References

[1] Shen Y *et al* 2021 Creation and control of high-dimensional multi-partite classically entangled light *Light: Sci. Appl.* **10** 50
[2] Guo G *et al* 2022 Topological band structure via twisted photons in a degenerate cavity *Nat. Commun.* **13** 2040
[3] Garcia-Gracia H *et al* 2017 Enhanced sensitivity at higher-order exceptional points *Nature* **548** 187–91
[4] Fu Z, Yang L, Li F, Mao W and Li Y 2024 Exceptional-point-enhanced phase sensing *Sci. Adv.* **10** eadl5037
[5] Su J, Goldberg A F G and Stoltz B 2016 Label-free detection of single nanoparticles and biological molecules using microtoroid optical resonators *Light Sci. Appl.* **5** e16001
[6] Zhong Q, Christodoulides D and El-Ganainy R 2018 Sensing with exceptional surfaces in order to combine sensitivity with robustness *Phys. Rev. Lett.* **122** 153902
[7] Lei F *et al* 2020 Experimental realization of sensitivity enhancement and suppression with exceptional surfaces *Laser Photon. Rev.* **15** 2000569
[8] Zhao Q *et al* 2016 Broad-bandwidth near-shot-noise-limited intensity noise suppression of a single-frequency fiber laser *Opt. lett.* **41** 1333–5
[9] Feng Z *et al* 2018 Noise-sidebands-free and ultra-low-RIN 1.5 Î single-frequency fiber laser towards coherent optical detection *Photon. Res.* **6** 326–31
[10] Miri M A and Alu A 2019 Exceptional points in optics and photonics *Science* **363** eaar7709
[11] Özdemir ŞK, Rotter S, Nori F and Yang L 2019 Parity–time symmetry and exceptional points in photonics *Nat. Mater.* **18** 783–98
[12] Bender C M and Boettcher S 1998 Real spectra in non-Hermitian Hamiltonians having $\mathcal{PT}$ symmetry *Phys. Rev. Lett.* **80** 5243–6

[13] Bender C M, Berry M V and Mandilara A 2002 Generalized PT symmetry and real spectra *J. Phys. A: Math. Gen.* **35** L467
[14] Bender C M 2007 Making sense of non-Hermitian Hamiltonians *Rep. Prog. Phys.* **70** 947
[15] Konotop V V, Yang J and Zezyulin D A 2016 Nonlinear waves in $\mathcal{PT}$-symmetric systems *Rev. Mod Phys.* **88** 035002
[16] Zhou X *et al* 2018 Optical lattices with higher-order exceptional points by non-Hermitian coupling *Appl. Phys. Lett.* **113** 101108
[17] Gupta S K *et al* 2020 Parity-time symmetry in non-Hermitian complex optical media *Adv. Mater.* **32** 1903639
[18] Wiersig J 2020 Review of exceptional point-based sensors *Photon. Res.* **8** 1457–67
[19] Meng H, Ang Y S and Lee C H 2024 Exceptional points in non-Hermitian systems: applications and recent developments *Appl. Phys. Lett.* **124** 060502
[20] Ding Q *et al* 2021 Parity-time symmetry in parameter space of polarization *APL Photonics* **6** 076102
[21] Lawrence M *et al* 2014 Manifestation of *PT* symmetry breaking in polarization space with terahertz metasurfaces *Phys. Rev. Lett.* **113** 093901
[22] Wang J, Shen Y, Yu X, Zou L, Ouyang S and Deng X 2021 Active control of parity-time symmetry phase transition in terahertz metasurface *Phys. Lett. A* **400** 127304
[23] Bisson J and Nonguierma Y C 2020 Single-mode lasers using parity-time-symmetric polarization eigenstates *Phys. Rev. A* **102** 043522
[24] Konotop V V and Zezyulin D A 2018 Odd-Time reversal $\mathcal{PT}$ symmetry induced by an anti-$\mathcal{PT}$-symmetric medium *Phys. Rev. Lett.* **120** 123902
[25] Zhang X L, Jiang T and Chan C T 2019 Dynamically encircling an exceptional point in anti-parity-time symmetric systems: asymmetric mode switching for symmetry-broken modes *Light: Sci. Appl.* **8** 88
[26] Ge L and Türeci H E 2013 Antisymmetric $\mathcal{PT}$-photonic structures with balanced positive- and negative-index materials *Phys. Rev. A* **88** 053810
[27] Wu J H, Artoni M and La Rocca G C 2014 Non-Hermitian degeneracies and unidirectional reflectionless atomic lattices *Phys. Rev. Lett.* **113** 123004
[28] Peng P *et al* 2016 Anti-parity–time symmetry with flying atoms *Nat. Phys.* **12** 1139–45
[29] Wu J H, Artoni M and La Rocca G C 2015 Parity-time-antisymmetric atomic lattices without gain *Phys. Rev. A* **91** 033811
[30] Xu H S and Jin L 2021 Coupling-induced nonunitary and unitary scattering in anti-$\mathcal{PT}$-symmetric non-Hermitian systems *Phys. Rev. A* **104** 012218
[31] Yang F, Liu Y C and You L 2017 Anti-$\mathcal{PT}$ symmetry in dissipatively coupled optical systems *Phys. Rev. A* **96** 053845
[32] Choi Y, Hahn C, Yoon J W and Song S H 2018 Observation of an anti-PT-symmetric exceptional point and energy-difference conserving dynamics in electrical circuit resonators *Nat. Commun.* **9** 2182
[33] Kuchment P A 1982 Floquet theory for partial differential equations *Russian Math. Surveys* **37** 1
[34] Oka T and Kitamura S 2019 Floquet engineering of quantum materials *Annu. Rev. Condens. Matt. Phys.* **10** 387–408
[35] Brunel M, Emile O, Alouini M, Le Floch A and Bretenaker F 1999 Experimental and theoretical study of longitudinally monomode vectorial solid-state lasers *Phys. Rev. A* **59** 831–40
[36] Huang Y *et al* 2023 Linear polarization emission of Yb:YAG laser via polarization mode frequency locking *Infrared Phys. Technol.* **128** 104516